Microprocessor-Controlled Eddy Current Measuring System for Qualitative On-Site Testing

Mayez Al-Mouhamed

Department of Computer Engineering
King Fahd University of Petroleum and Minerals (KFUPM)
31261 Dhahran, Saudi Arabia

Abstract: A portable microprocessor-controlled eddy current measuring system to automate qualitative testing of metallic bodies. The system embodies automatic setting of operating frequencies, self-tuning, and measures variations in impedance of the sensing coil that correspond to defects or variation of the material under test. Small changes in signal phase and amplitude are detected by fast hardware which is controlled by a microprocessor. Evaluation shows clear detection of defects upon phase analysis.

MICROPROCESSOR-CONTROLLED EDDY CURRENT MEASURING SYSTEM FOR QUALITATIVE ON-SITE TESTING

Mayez Al-Mouhamed*

Computer Engineering Department
King Fahd University of Petroleum & Minerals
Dhahran, Saudi Arabia

الخلاصـــة :

يناقش هذا المقال نظام الحاسب الأصغر لأتمتة عمليات القياس النوعي لتيار (آدي) في السطوح المعدنية ، ويتضمن هذا النظام تصميم أتمتة تعيين التواتر المطلوب في العمليات والتحسين الذاتي ، ويسمح النظام بقياس التغيرات الكهربائية في وشيعة Coil استشعار مما يؤدي الى قياس الخلل أو التغيرات في المادة المعدنية المختبرة ، وتقاس تغيرات الطور والسعة بواسطة تصميم يتميز بالسرعة ويتحكم به حاسب آلي صغير . ويفيد تقييم النتائج الى إمكانية كشف واضح للخلل بواسطة تحليل الطور .

ABSTRACT

A portable microprocessor-controlled eddy current measuring system to automate qualitative testing of metallic bodies. The system embodies automatic setting of operating frequencies, self-tuning, and measures variations in impedance of the sensing coil that correspond to defects or variation of the material under test. Small changes in signal phase and amplitude are detected by fast hardware which is controlled by a microprocessor. Evaluation shows clear detection of defects upon phase analysis.

*Address for correspondence:
KFUPM Box No. 787
King Fahd University of Petroleum & Minerals
Dhahran 31261
Saudi Arabia

Mayez Al-Mouhamed

MICROPROCESSOR-CONTROLLED EDDY CURRENT MEASURING SYSTEM FOR QUALITATIVE ON-SITE TESTING

1. INTRODUCTION

For many types of equipment and installations, qualitative on-site testing is highly desirable for early detection of deformation or corrosion affecting the metallic parts. Several methods [1, 2] of nondestructive testing (NDT) of metallic bodies using induced eddy currents have been investigated. Wait [3] proposed the induction of an eddy current by means of a solenoid carrying an alternating field that encircled a cylindrical sample. His analytical formulation showed that the solenoid impedance was a complex function depending on the conductivity and magnetic permeability of the sample. Another configuration, consisting of an excitation coil placed close to the sample, has been studied by Girgis and Bastrawros [4]. In this case, the impedance of the excitation coil was more sensitive to the product of conductivity and magnetic permeability over a range of frequencies, depending on the sample thickness. In his work, Sabbagh [5] used a coil encircling a highly permeable core, such as a ferrite, to shape and concentrate the electromagnetic field, especially at higher excitation frequencies. His elegant derivation analytically describes the magnetic induction within the core, the driving-point impedance of the coil-core, and the induced eddy currents within a sample placed close to the coil-core.

Eddy current-based nondestructive testing is widely used in many areas. Commercially available systems are still essentially manual in terms of setting the operating modes, tuning the sensor, and classification of feature outputs. Self-tuning and automatic recognition are two desirable features for increasing the flexibility of NDT methods. The integration of microcomputers into industrial eddy current test lines has been investigated. Stumm [6] investigated the required system structure at different functional levels with the objective of achieving reliable testing and a low rejection rate. One important problem is the setting of operating modes, which involves automatic monitoring of different test frequencies or different-shaped coils, together with control of the external mechanics to save the operator cost and time. Another aspect is signal evaluation and the generation of a reliable decision based on the analysis of the signal shape and potential classification of defects. To achieve that degree of flexibility and automation, Stumm proposed a testing system architecture which consists of three processors operating in parallel by means of an (IEC) bus. Simard *et al.* [7] proposed an automatic recognition method based on analysis of the image of defects obtained by scanning. Their method allowed an 80% rate of success in differentiating between the crack-shaped defects and any others.

This paper proposes a method for setting operating modes and self-tuning of the eddy current sensor for on-site qualitative NDT. The system embodies automatic setting of operating frequencies, self tuning, and measures variations in impedance of the material under test. The system detects small variations in the characteristics of the tested material by monitoring the phase and amplitude of the sensor output. The sensor design involves two independent steps:

1. The design aspects of eddy current sensors, in order to achieve reasonable sensitivity, and their theoretical backgrounds.
2. The use of some interesting results of filter theory, such as the generation of significant phase and amplitude variations in response to frequency shifting.

The system is composed of two sections. The first contains a programmable function generator and the digital electronics to measure the sensor output, *i.e.*, phase and amplitude of the sensing circuit output. The second part consists of a microprocessor-based system to perform automatic mode-frequency searching and setting, and to manage on-site data processing such as reading, filtering, displaying, and recording results.

The hardware is optimized to limit the power consumption to 1.2 A. The use of a microprocessor enables the system to manage the testing operations and offers greater flexibility of use and development. The results obtained are presented and discussed in the evaluation of the design performance.

2. IMPEDANCE OF AIR-CORED COILS

An important feature in the design of an eddy current-based sensor is the coil impedance and its dependency upon the coil dimensions. Dodd and Deeds' [8] formulation of the impedance for an air-cored coil allows numerical integration of the

impedance formula. The impedance change ($\Delta Z = Z - Z_o$) represents the variation of impedance when the coil is placed close to the sample (Z) and in free air (Z_o). The modeled coil C2 (Figure 1) has length L, inner radius R_1, outer radius R_2, and H as the distance between the coil and the sample. If the outer radius R_2 is used as normalizing factor with the dimensionless parameters $1 = L/R_2$, $r = R_1/R_2$, $h = H/R_2$, and normalized frequency $f = \omega\mu_o\sigma R_2^2$, using Dodd and Deeds' formulation, ΔZ will be:

$$\Delta Z = j\pi\omega\mu_o R_2 \left[\frac{N}{1(1-r)}\right]^2 \times \int_o^\infty \left[\frac{I(t,tr)}{t^3}\{\exp(-th) - \exp(-t(h+1)\}\right]^2 \times \eta(t,f)\,dt\,, \quad (1)$$

where ω is the angular frequency, μ_o is the magnetic permeability of the vacuum, σ is the conductivity of the sample, N is the number of turns, $j = \sqrt{(-1)}$, $I(t, tr)$ is a definite integral of the first-order Bessel function $J_1(x)$:

$$I(t, tr) = \int_{tr}^{t} J_1(t) \quad (2)$$

and $\eta(t,f)$ is a complex function:

$$\eta(t,f) = \frac{t - \sqrt{(t^2 + jf)}}{t + \sqrt{(t^2 + jf)}}\,. \quad (3)$$

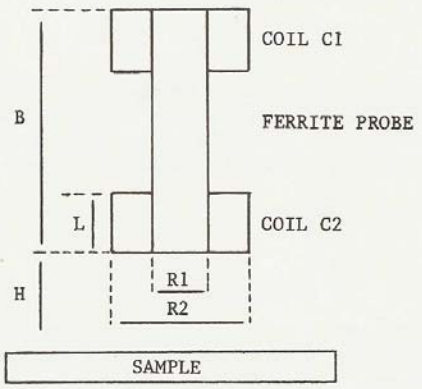

Figure 1. Detail of the Sensor.
Here $R_1 = 6$ mm, $R_2 = 12$ mm, $L = 4$ mm, and $B = 60$ mm. The inner and outer radii are R_1 and R_2 respectively, and L is the coil length. The normalized length $l = L/R_2$ should be kept below 0.5 in order to achieve reasonable sensitivity. Here, $l = 0.33$. The ratio of radii $r = R_1/R_2$ does not significantly affect the sensitivity of the probe coil.

Using computer simulation, Skopal *et al.* [9] carried out the integration of Equation (1) and obtained impedance diagrams which show the effect of changing the length l, normalized frequency f, and radius r. The analysis of these diagrams in terms of the various influencing parameters allows the following observations:

1. The inner radius r has only slight effect on sensitivity and consequently the ratio of radii does not significantly affect the sensitivity of the probe coil.
2. An increase of the length l is virtually an increase of the spacing between the coil and the sample, which in turn causes a decrease of the average sensitivity. When l increases from 0.1 to 1, both components of ΔZ, the relative reactance ($\Delta\omega L/\omega L$) and relative resistance ($\Delta R/\omega L$) strongly decrease by a 2.5 factor in the normalized frequency range ($f = 5-5000$). The normalized length l should be kept below 0.5 in order to achieve reasonable sensitivity.

In conclusion, significant sensitivity can be achieved using short coils.

3. COIL ENCIRCLING FERRITE CORE

The use of ferrite-cored coils increases the sensitivity of impedance [10] because of a considerable increase in flux density as a result of the relatively high magnetic permeability, which is between 40 μ_o and 1000 μ_o. Ferrites have the advantage of being electrically low conductors (10^{-9} to 10^{-3} Sm^{-1}) and consequently eddy currents are virtually absent in the ferrite core. Here, the ferrite core is essentially used to shape and concentrate the magnetic flux and to extend the sensing from the position of the sensing coil down to the surface of the tested material.

4. PRINCIPLE AND DESIGN

Defects in the sample produce variations in the penetration of the excitation field and consequently the eddy field is significantly modified by the electrical and geometrical characteristics of the defect. The system is designed to sense variations of impedance caused by the variation of the eddy field emitted by the sample. The designed system consists of an excitation coil (C1) and a sensing coil (C2), both of which are tightly coupled at opposite ends of a ferrite core [Figure 2]. Coils C1 and C2 have inductance (L_1) and (L_2) respectively and mutual coupling $\{M_2 = \sqrt{(L_1 L_2)}K_2\}$, K_2 is the coupling constant.

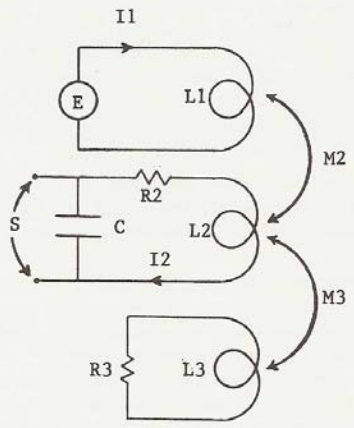

Figure 2. Equivalent Circuit of the Sensor. Where: C1 is the excitation circuit ($L_1 = 0.001$ H), *C2 is the sensing circuit, S is the sensor output* ($L_2 = 0.001$ H, $R_2 = 0.8$ *Ohms, and C is variable), C3 is a simple electric model for the tested metallic body,* M_2 *is the mutual coupling between inductance* L_1 *and* L_2 ($M_2 = \sqrt{(L_1 L_2)K_2}$), K_2 *is the coupling factor,* M_3 *is the mutual coupling between inductance* L_2 *and* L_3 ($M_3 = \sqrt{(L_2 L_3)K_3}$).

The sensing coil is perpendicularly adjacent to the sample. The excitation coil is fed with an alternating voltage (E), the sensing coil output (S) results from the combination of the excitation and the eddy field induced in the metallic body under test. The sensing coil inductance is mounted in parallel with a capacitor (C), and the resulting sensor circuit is therefore an (RLC) network. The sample impedance can be modeled [11, 12] by using a resistance (R_3) and an inductance (L_3) which is coupled to the sensing coil inductance L_2 by mutual coupling $\{M_3 = \sqrt{(L_2 L_3)K_3}\}$.

4.1. Principle of the Sensor

The excitation coil C1 is fed with an alternating voltage E and produces an alternating magnetic field which is mainly oriented parallel to the ferrite axis. When this field is projected on a nonmagnetic electrically conducting body, eddy currents are induced in that body flowing in a plane perpendicular to the excitation magnetic field and causing partial cancellation. As coil C2 is traversed by the resulting magnetic field, its impedance changes. Thus, monitoring of the electric signals generated by coil C2 allows one to monitor the resulting magnetic flux in the ferrite core. When the sensor passes over a defect, the eddy currents are altered depending on the geometric, electric, and magnetic characteristics of the defect. This results in a change of the resulting flux which in turn causes a change in the impedance of the sensing coil.

Eddy currents flowing in the sample produce a magnetic field which opposes the excitation field, thus reducing that field and causing a decrease in eddy current density with increasing depth. The decrease in eddy current density is exponential with increasing depth [13]. The standard depth of penetration or skin depth (δ) is defined as the depth at which eddy current density decreases to 36.8% of the surface density. The skin depth is defined by $(\delta = 1/\sqrt{\{(\pi f \mu_o \sigma)\}})$. Thus, lower frequencies produce greater depth penetration. Sensitivity to defects depends on defect depth because current density at (3δ) is only 5% of surface density, and therefore this effect imposes a limit on defect detection.

4.2. Transfer Function of the Sensor

Using the circuit of Figure 2, three differential equations can be written for coils C1, C2, and C3. Assuming that initially all currents are zero and replacing the differential operator (d/dt) with the Laplace complex frequency variable (p), one gets the following equation:

$$E = \frac{Z_1}{pM_2}\left[Z_2 - \frac{(pM_2)^2}{Z_1} - \frac{(pM_3)^2}{Z_3}\right] \cdot I_2 \,. \quad (4)$$

Where Z_1, Z_2, and Z_3 are the impedance of circuits C1, C2, and C3 respectively, I_2 is the AC current circulating in C2. The transfer function ($H(p)$) between sensor output S and the excitation E becomes:

$$H(p) = \frac{S(p)}{E(p)} = \frac{M_2}{C}\left(\frac{1}{Z_1 Z_2 - (pM_2)^2 - (pM_3)^2 Z_1/Z_3}\right) . \quad (5)$$

The impedance $Z_1 Z_2 - (pM_2)^2$ is a second order polynomial. Given the characteristics of impedances Z_1 and Z_3, one gets:

$$\frac{Z_1}{Z_3}(pM_3)^2 = L_1 L_2 K_3^2 \frac{p^3}{p + R_3/L_3} \,. \quad (6)$$

The function $Z_1/Z_3(pM_3)^2$ can be approximated by the following second order polynomial if $R_3/\omega L_3 \ll 1$ in the operating range of frequencies:

$$\frac{Z_1}{Z_3}(pM_3)^2 = L_1L_2K_3^2\left[p^2 - \frac{R_3}{L_3}p + \left(\frac{R_3}{L_3}\right)^2\right]. \quad (7)$$

The theory of Artificial Transmission Line for plane wave conditions can be used to model the metal conductor under test [12] and thus provides an approximate value of $R_3/\omega L_3$. It is known from this theory that the series impedance of the equivalent line is $Y = j\omega\mu$ and the shunt admittance $X = \sigma$. This leads to $R_3/\omega L_3 = 1/\omega\sigma\mu$. The term $\sigma\mu$ is on the order of 17.6 (brass), 42.7 (aluminum), and 71.6 (copper). Thus, $R_3/\omega L_3 \ll 1$ is justified, at least, for good metallic conductors.

Given the impedance Z_1, Z_2, and Z_3, $H(p)$ can be written as follows:

$$H(p) = \frac{H}{p^2 + \frac{\omega_1}{Q}p + \omega_1^2}. \quad (8)$$

Here H, ω_1/Q, and ω_1 are given by the Equations (9–11):

$$H = \frac{K_2}{C\sqrt{(L_2L_2)}\,(1 - K_2^2 - K_3^2)} \quad (9)$$

$$\frac{\omega_1}{Q} = \frac{R_2 + L_2R_3K_3^2/L_3}{L_2(1 - K_2^2 - K_3^2)} \quad (10)$$

$$\omega_1^2 = \frac{1/C - L_2(R_3K_3/L_3)^2}{L_2(1 - K_2^2 - K_3^2)}. \quad (11)$$

Thus, $H(p)$ can be approximated to a low-pass filter with a cutoff frequency ω_1. In the passband, a peak of gain, $G = HQ/\omega_1$, appears at frequency $\omega = \omega_1\sqrt{(1-\frac{1}{2}Q^2)}$. A detailed description of this filter can be found in Reference [14]. The phase response is governed to a large extent by the factor Q. For $Q > 5$, the phase udergoes a rapid shift of 180 degrees about ω_1. Given the parameter of this design (Figure 2), Q ranges [6, 600] for frequencies of 1 kHz to 100 kHz.

Let ω_o be the cutoff frequency of $H(p)$ when the sensor is placed in free air, *i.e.*, K_3 is zero. Using Equation (11), we have:

$$\omega_o^2 = \frac{1}{CL_2(1 - K_2^2)}. \quad (12)$$

Assume the sensor is placed close to the sample and frequency $\omega = \omega_1$ is set, thus the phase will be nearly $-\pi/2$. When the sensor is scanning a defect, the sample parameters (R_3, L_3) are changed and this causes variations $(\Delta\omega_1)$ on the characteristic frequency ω_1. For small variations of R_3/L_3, one gets:

$$\omega_1\Delta\omega_1 = \frac{-K_3^2}{1 - K_2^2 - K_3^2}\,\frac{R_3}{L_3}\Delta\left(\frac{R_3}{L_3}\right). \quad (13)$$

Combining Equations (12) and (13), the relative variation of ω_1 can then be expressed as function of relative variations of R_3 and L_3:

$$\frac{\Delta\omega_1}{\omega_1} = \left[1 - \frac{\omega_o^2}{\omega_1^2}\right]\left[\frac{\Delta R_3}{R_3} - \frac{\Delta L_3}{L_3}\right]. \quad (14)$$

The excitation frequency is constant $(\omega = \omega_1)$, thus the variation in the characteristic ω_1 causes phase and amplitude variations in the transfer function $H(p)$, *i.e.*, variation in the amplitude and phase of the output signal S. In accordance with the properties of the transfer function $H(p)$, the phase variations are maximum when the excitation frequency is set to ω_1 (Equation 11) while the sensor is placed close to the sample. Figure 3(*a*) shows the resulting phase variations (ΔP) in response to variations in the characteristic frequency ω_1.

An interesting feature of this network is that the phase difference (P), between the excitation signal E and the sensor output S, and the amplitude of S significantly change at frequencies around the resonant frequency ω_1. The characteristics (ω_1, Q,

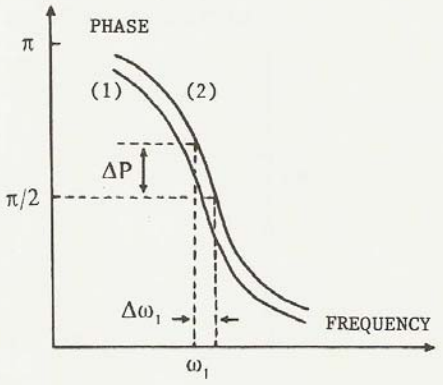

Figure 3(a). Phase Variations versus *Variation in the Cutoff Frequency.*
The curves (1) and (2) represent the phase characteristics when the sensor is placed adjacent to the sample and close to a defect respectively. A variation $\Delta\omega_1$ in the filter characteristic (cutoff frequency) produces large phase variations (ΔP) if the excitation frequency (ω) is set to ω_1 while the sensor is adjacent to a reference point of the sample.

and H) are functions of the equivalent impedance Z_3 of the sample and the spacing between the sensor and the sample, *i.e.*, parameter K_3. Thus, variation of the phase with respect to the setting of ω_1 while the sensor is close to the sample, can be interpreted as being due to change in the sample's characteristics when the scan conditions are maintained.

Assume the frequency is set to ω_1 while the sensor is placed close to the sample. In this case, the phase P is nearly $-\pi/2$. When the sensor is over a defect, the sample impedance Z_3 changes causing a shift in the characteristic frequency ω_1 of $H(p)$. As a result, significant variation of the phase P will be obtained because for ω_1 the phase sensitivity *versus* frequencies ($\Delta P/\Delta\omega$) is maximum according to the properties of the transfer function $H(p)$ and the effect of high Q factor.

Figure 3(b) shows the plot of the phase *versus* the period ($T_1 = 2\pi/\omega_1$). Curve 1 is obtained when the sensor is placed in free air and $f_o = 26315$ Hz ($T_o = 38\ \mu s$). Curve 2 is obtained when the sensor is placed over an iron sheet. Curve 3 is obtained when the sensor is close to an aluminum sheet the geometrical features of which are described in Section 6, on evaluation. In this case, the phase curve is shifted by a frequency $\Delta f = 2670$ Hz ($f_1 = 28985$ Hz) with respect to f_o which is obtained when the sensor is placed in free air. Curve 4 is obtained when the sensor is placed over a deep scratch in the aluminum sheet (Defect 3 in Section 6). This defect causes a slight shift of the phase (Curve 4) which corresponds to a frequency change of $\Delta f = 331$ Hz (or $\Delta T = 0.4\ \mu s$). In this range of frequencies, the setting of the system to frequency f_1 allows measurement of the largest amount of phase variations with the aluminum sheet because $\Delta P/\Delta f$ is maximum around f_1.

On the other hand, Equation 14 indicates that equal relative variations in the resistive and reactive components of the sample impedance will not produce variations in the transfer function characteristics ($H, \omega_1/Q, \omega_1$) of $H(p)$ because of mutual cancellation of these components. This effect does not affect the sample's contribution, *i.e.*, term $(pM_3)^2/Z_3$ in Equation 4, which remains constant in this case.

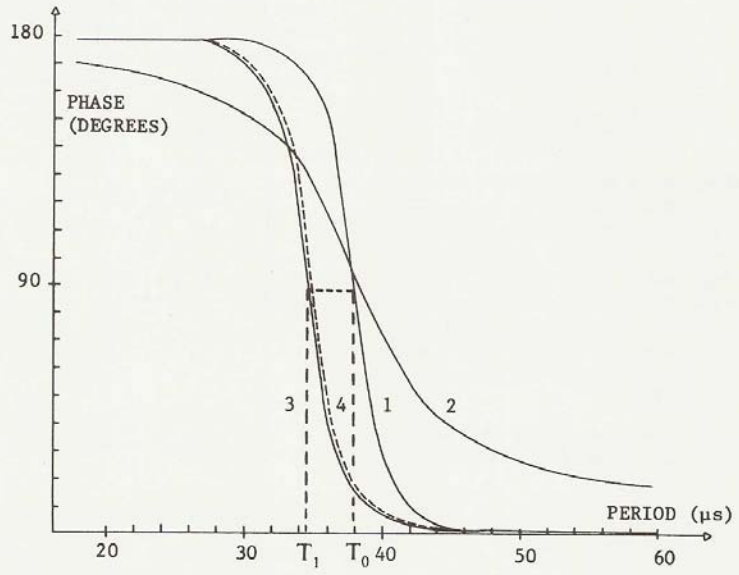

Figure 3(b). *Phase Characteristics* versus *the Period of the Excitation Frequency.*
The curves refers to phase shift when the sensor is: 1. In free air; 2. Close to an iron sheet; 3. Close to an aluminum sheet and; 4. Close to a defect in the aluminum sheet. In this case the defect produces a translation of the phase characteristic.

4.3. Programmable Function Generator

A programmable function generator (Figure 4) is used to feed the coil C1. The excitation frequency (f) is controlled by a microprocessor using the relation ($f = F/2N$), where $F = 32$ MHz and N is a 16-bit integer number. Thus, the frequency resolution is ($\Delta f = f/(N+1)$). As pointed out in Section 4.2, the quality factor Q should satisfy ($Q > 5$) to ensure abrupt change of the phase around the frequency f_1. Given the parameters of coils C1 and C2, this condition can be satisfied for $f \geq 1$ kHz ($N \leq 16 \times 10^3$).

On the other hand, if at least a relative resolution $\Delta f/f = 0.01$ is to be achieved on the generated frequencies, then the highest frequency should not exceed $f = 161$ kHz ($N \geq 99$). Thus, the generated frequencies have the range [1 kHz−161 kHz] in our design.

4.4. Design and Measurements

The architecture of the controller is organized around a 16-bit microprocessor (8086-2) running at 8 MHz. The processor resource consists of CMOS memories, communication devices, and an I/O system to set the function generator, read the sensor data, control a 20-key keyboard, and display data using a 6-digit numeric display. The I/O system, which is the crucial part of the electronics (Figure 4), is dedicated for controlling the sensor operations. This system

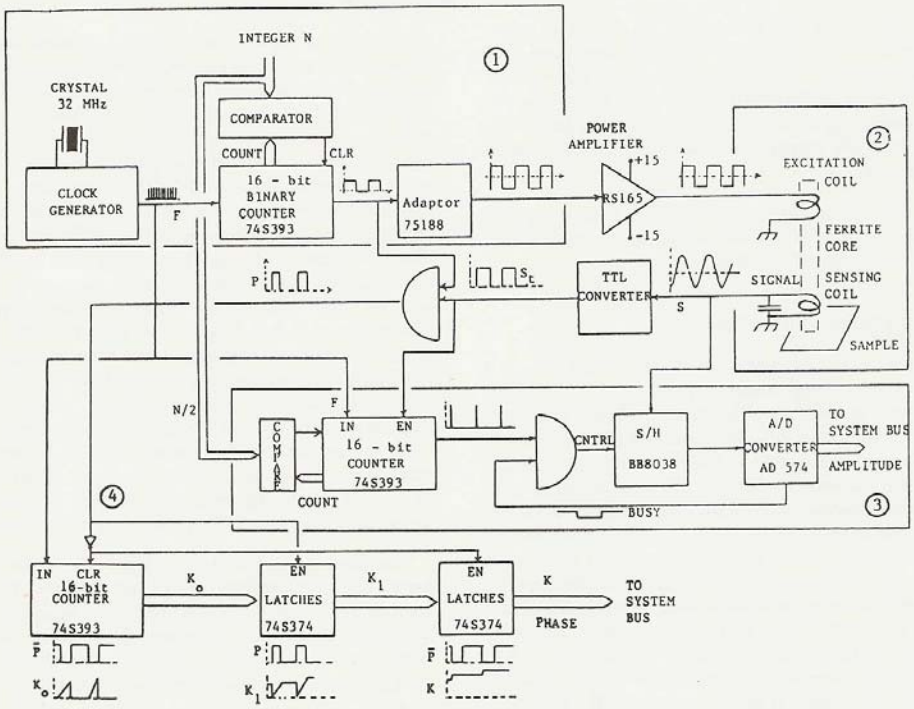

Figure 4. Hardware for Controlling the Sensor Operations.

1. A programmable function generator is designed using fast TTL components to allow accurate ($\Delta f/f \leq 0.01$) setting of the excitation frequencies in the range (1 kHz−158 kHz); 2. The sensor probe consists of an excitation coil and a sensing coil, both of which are loosely coupled at opposite ends of a ferrite core; 3. Hardware to measure the amplitude: synchronizes latching of the amplitude of signal S coinciding with the half period time; 4. Hardware to measure the phase: the TTL signal resulting from ANDing the excitation signal with the sensing signal, is used to enable a fast counter to measure the phase. This hardware provides the digital approximation of the phase with an error ($\varepsilon \leq 31.25$ ns).

was designed using fast TTL devices which naturally have higher power consumption than MOS devices. The advantage of this method is to provide the digital form of the phase information with the shortest hardware latency which is on the order of 10 ns, compared with the converter delay (5−10 μs).

The phase difference, between the excitation E and the sensing coil output S, is measured using a digital counter rather than a phase locked-loop circuit. This has the advantage of generating digital output and also no converter will be required. However, it has the drawback of limiting the smallest phase difference which can be detected to $2\pi f/F\ rd$, where f and F are the frequencies of the excitation and the source (32 MHz) respectively.

The period of the sensing coil output S corresponds to a time $(T = 2N/F)$. Therefore, the amplitude of S corresponds to $S(N/2)$. The value of $S(N/2)$ is latched by the electronics every time the counter output is $N/2$. Here, the amplitude $S(N/2)$ is analog in nature and consequently a converter is required.

This design allows the system to work using only 1.2 A against 4.3 A on similar commercial microprocessor-based systems.

5. SYSTEM OPERATIONS

Given the parameters of circuits C1 and C2, ω_o is evaluated using Equation (12), *i.e.*, the sensor is placed in free air. The setting of this frequency $(N_o = \text{Integer}(\pi.F/\omega_o))$ results in a phase difference $P = -\pi/2$ according to the characteristics of $H(p)$. When the sensor is placed adjacent to the sample, the parameters of $H(p)$ are slightly modified because of the appearance of terms K_3 and the impedance Z_3. Consequently, the transfer function parameters H, Q, and ω_1 are changed according to the approximate model given in Equations (9−11). The value of the shifted frequency ω_1 is found by searching around the previous frequency ω_o. Thus, tuning of the sensor is achieved by setting the frequency ω_1 for which the phase is again $P = -\pi/2$. We note here that the phase slop $(\Delta P/\Delta f)$ is maximum according to the definition of the low-pass function $H(p)$.

When the sensor passes over a defect, the sample impedance Z_3 is changed together with the characteristic ω_1, also slightly affecting the parameters H and Q, leading to a significant phase variations.

6. EVALUATION

In order to evaluate the system and demonstrate its capabilities, five feature-defects have been designed on aluminum sheets 50 cm × 35 cm and 1.2 mm thick. The feature-defects are as follows:

1. a butt joint, 0.2 mm wide between two sheets;
2. a linear cut 0.4 mm wide, 1 mm deep, and 15 mm long;
3. a deep scratch, 0.2 mm wide, 0.35 mm deep, and 10 mm long;
4. a rectangular slot 1.5 mm wide, 0.3 mm deep, and 350 mm long; and
5. a scratch 0.7 mm wide, 0.1 mm deep, and 100 mm long.

To test these features at various frequencies, four values of the sensor coil capacitor have been selected for generating resonant frequencies at 2264 Hz, 5000 Hz, 14720 Hz, and 25974 Hz. The setting of the frequency mode was automatically achieved by applying the procedure described in Section 5. For example, with a capacitor of 0.033 μF the frequency f_o is 25974 Hz when the sensor is placed in free air and the phase is −90 degrees. The amplitude of S is 36.4 V. When setting the sensor adjacent to the aluminum sheet, the amplitude of S drops to 9.4 V and the phase becomes −9.35 degrees. The system adjusts the excitation frequency so that the phase is again −90 degrees. This is achieved for a frequency $f_1 = 29205$ Hz, and the amplitude of S is 24.6 V. Assume the sensor is placed on defect 1, then the amplitude drops to 14.4 V and the phase becomes −148 degrees, *i.e.*, a phase variation of −58 degrees. This shows how the transfer function $H(p)$ is dependent on the characteristics of the aluminum sheet, *i.e.*, impedance Z_3, when using this design.

The phase variations shown in Figures 5−9, correspond to cross-sectional scans of features 1−5 respectively. Phase variations are plotted against the linear coordinates of the scans. Each figure has labeled curves 1−4 that correspond to the scan of a feature at the four above-mentioned frequencies.

The curves clearly show that the amplitude of the phase variation significantly increases with the geometric dimensions of the defect. When the eddy field is absent, *i.e.*, when the sensor is placed in free air, the phase is greatly increased. The increase in phase (Figures 5 and 6) is attributed to a loss in the eddy field, *i.e.* a portion of the excitation field is lost

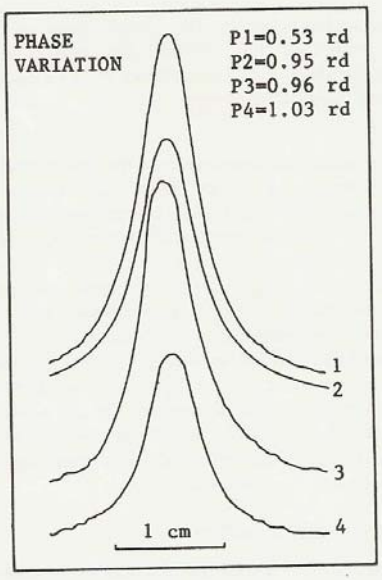

Figure 5.

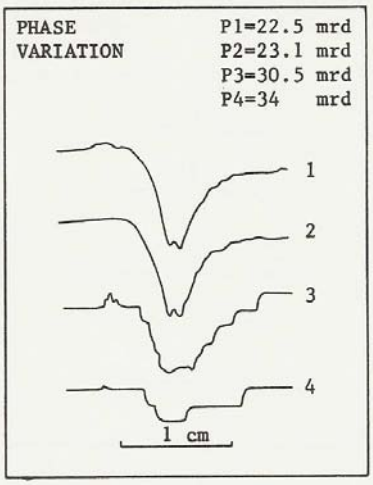

Figure 7.

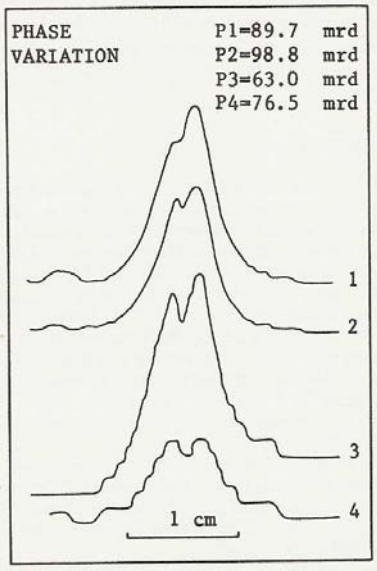

Figure 6.

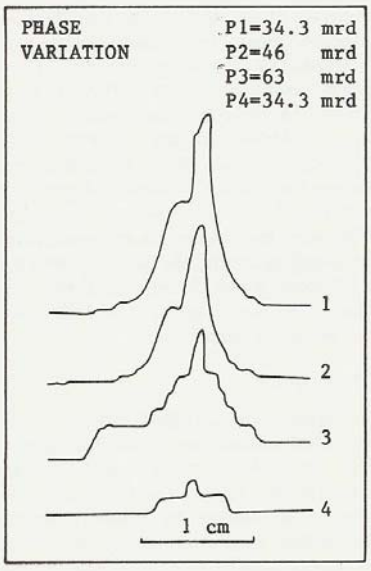

Figure 8.

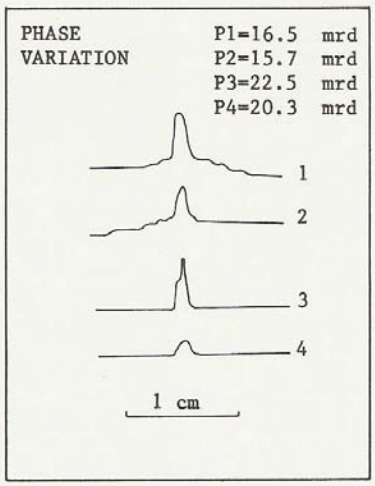

Figure 9.

in the gap and the eddy field emitted by the defect borders is diminished because of the redistribution of eddy currents on each border.

In the case of a defect having a small geometric characteristic (Figure 7–9), smaller phase variation are observed at all the testing frequencies. However, the phase resolution is not sufficient at higher frequencies. To overcome this problem, the source frequency (32 MHz) should be higher. Consequently, faster switching electronics will be required to measure the smaller difference of phase, in the order of 5 ns, due to the above excitation frequencies. The use of low frequencies allows the excitation field to deeply penetrate the sample. The effect on phase is global; however the sensor gives a good detection of defects (Figures 7 and 9) that have reduced geometric dimensions.

7. CONCLUSION

A microprocessor-controlled eddy-current measuring system for qualitative on-site testing has been designed and implemented. Interesting features of this design are the easy automatic setting of testing frequencies, self-tuning of sensing capabilities, and automated measurements by means of the microprocessor-based system. In this design, the use of a single source of frequency has greatly improved the stability of measurements. The design of separate hardware for the measurement of phase and amplitude has released the microprocessor from low-level tasks and allows it to be used for setting measurement conditions and on-line data management.

Evaluation demonstrates that the system performs according to the design objectives. At lower frequencies, NDT-based eddy current investigation is certainly a rich source of information about defects or fatigue effects that modify the material's resistance. Defects having small geometric dimensions produce smaller changes in phase and amplitude and consequently their detection is conditioned by the use of higher clock frequencies and appropriate electronics. The system could also be improved by implementing software for noisy environments. The use of the FFT and its inverse transforms on the portable module could eliminate the effects of the surrounding noisy electromagnetic environment.

ACKNOWLEDGEMENT

The author wishes to thank Dr. Mohammad Al-Suwaiyel, Dean College of Computer Science and Engineering at KFUPM, for his moral support. Thanks are due to Mr. Jean-Marie Tizon of Computer Engineering Department (KFUPM) for his valuable contribution in the implementation of the hardware section. The author thanks the Research Institute at KFUPM for partially supporting this research.

REFERENCES

[1] C. V. Dodd and W. E. Deeds, "In-Service Inspection of Stream-Generator Tubing by Multiple Frequency Eddy-Current Techniques", *ASTM Special Technical Publication 722*, ed. G. Birnbaum and G. Free. The American Society for Testing and Materials, 1981.

[2] G. Free, "High-Accuracy Conductivity Measurements in Nonferrous Metals", *ASTM Special Technical Publication 722*, ed. G. Birnbaum and G. Free. The American Society for Testing and Materials, 1981.

[3] J. R. Wait, "Electromagnetic Basis for Non-Destructive Testing of Cylindrical Conductors", *IEEE Transactions on Instrumentation and Measurement*, **IM-27** (1978), p. 235.

[4] G. Girgis and A. Bastawros, "Nondestructive Eddy Current Testing for the Measurement of Conductivity and Surface Buckling of Metallic Sheets", *IEEE Transactions on Instrumentation and Measurement*, **IM-35** (1986), p. 619.

[5] H. A. Sabbagh, "A Model of Eddy-Current Probes with Ferric Cores", *IEEE Transactions on Magnetics*, **MAG-23(2)** (1987), p. 1888.

[6] W. Stumm, "A Review of the Integration of Microcomputers into Eddy Current Test-Lines", *The British Journal of Non-Destructive Testing,* **26(3)** (1984), p. 154.
[7] P. Simard, P. Gaillard, and J. F. Chretien, "An Attempt at Automatization of an Eddy Current Nondestructive Testing", *Journal of Nondestructive Evaluation,* **5(3/4)** (1986), p. 109.
[8] C. V. Dodd and W. E. Deeds, "Analytical Solutions to Eddy-Current Probe-Coil Problems", *Journal of Applied Physics,* **39** (1968), p. 2829.
[9] I. Skopal, F. Tobias, and P. Ivanov, "Some Problems of Eddy Current Testing with Air-Cored Probe Coils", *NDT International,* **21(3)** (1988), p. 159.
[10] N. T. Hajian and J. Blitz, "Prediction of Impedance Components for Eddy-Current Probe Coils for Standardization", *NDT International,* **19(5)** (1986), p. 333.
[11] A. McNab and J. C. Hale, "Electromagnetic Crack Detection in Ferritic Steel", *Journal of Nondestructive Evaluation,* **4(3/4)** (1984), p. 165.
[12] H. L. Libby, *Introduction to Electromagnetic Nondestructive Test Methods.* New York: Wiley-Interscience, 1971, p. 154.
[13] G. Van Drunen and V. S. Cecco, "Recognizing Limitations in Eddy-Current Testing", *NDT International,* **17(1)** (1984), p. 9.
[14] F. W. Stephenson, *RC Active Filters Design Handbook.* New York: Wiley, 1985, p. 55.

Paper Received 8 May 1988; Revised 5 June 1989.